Supplement of Hydrol. Earth Syst. Sci., 27, 4453–4465, 2023
https://doi.org/10.5194/hess-27-4453-2023-supplement


Hydrology and Earth System Sciences
Open Access

*Supplement of*

# A pulse-decay method for low (matrix) permeability analyses of granular rock media

**Tao Zhang et al.**

*Correspondence to:* Qinhong Hu (huqinhong@upc.edu.cn)

## S1. Consideration of Non-linearity of Gas and Solutions for a Mixed Gas State

For gas flow, we can use a pseudo-pressure variable to linearize Eq. (2A) as $\mu$ and $c_t$ are functions of pressure. The pseudo-pressure $p_p$ is defined as (Haskett et al., 1988)

$$p_p = 2\int_{p_0}^{p} \frac{p}{\mu z} d\,p \tag{S1}$$

By combining Eq. (S1) with the ideal gas law, the pseudo-density may be expressed as

$$\rho_p = \frac{pM}{RT} = \frac{p^2 M}{\mu z RT} \tag{S2}$$

Because viscosity and compressibility do not change significantly (less than 0.7%) between 200 psi and atmospheric pressures, Eq. (S2) can be simplified to

$$\rho_p = \frac{p^2 M}{RT} \tag{S3}$$

Thus, the density change is replaced by the pseudo-density for a precise calibration by using pressure squared.

During the GPT experiment, different gases in the reference and sample cells may complicate the hydrodynamic equilibrium of gas, and consequently

the expression of transport phenomena, as the viscosity and gas compressibility are in a mixed state. Therefore, during the GPT experiment when a different gas exists between the reference and sample cells a, a mixed viscosity should be used after the gas in reference cell is released into the sample cell. The viscosity of mixture $\mu_{mix}$ under pressure in Eqs. (3a)-(3c) can be calculated from (Brokaw, 1968; Sutherland, 1895)

$$\mu_{mix} = \sum \frac{\mu_i}{1 + \frac{1}{y_i}\left(\sum_{\substack{j=1 \\ j\neq i}}^{n} B_{ij} y_j\right)} + \mu_p \tag{S4}$$

$B_{ij}$ is a correction parameter independent of gas composition and can be expressed as

$$B_{ij} = \frac{[1 + (\frac{\mu_i}{\mu_j})^{0.5} (\frac{M_j}{M_i})^{0.5}]^2}{2\sqrt{2}(1 + \frac{M_j}{M_i})^{0.5}} \tag{S5}$$

in which $\mu_p$ is the correction term for the viscosity variation as its changes with pressure and given by

$$\mu_p = 1.1 \times 10^{-8}\left(e^{1.439\rho_{rm}} - e^{-1.111{\rho_{rm}}^{1.858}}\right) \times {M_m}^{0.5} \cdot \frac{{P_{cm}}^{\frac{2}{3}}}{{T_{cm}}^{\frac{1}{6}}} \tag{S6}$$

## S2. Gas Transport in GPT

From Eq. (2A), the transport of gas in the GPT with the "unipore" model under a small pressure gradient in a spherical coordinate system with laminar

flow is based on the Darcy-type relation. Because the transfer rate of the fluid is proportional to the concentration gradient, this process can be expressed as:

$$\frac{\partial \rho_p}{\partial t} = \frac{k}{c_t \phi_f \mu}\left(\frac{2}{r}\frac{\partial \rho_p}{\partial r} + \frac{\partial^2 \rho_p}{\partial r^2}\right) \tag{S7}$$

We set

$$k_s = \frac{k}{\mu} \tag{S8}$$

$$K_a = \frac{k_s}{c_t \phi_f} \tag{S9}$$

Then, Eq. (S7) becomes:

$$\frac{\partial \rho_p}{\partial t} = K_a\left(\frac{2}{r}\frac{\partial \rho_p}{\partial r} + \frac{\partial^2 \rho_p}{\partial r^2}\right) \text{ or } \frac{\partial}{\partial t}(\rho_p r) = K_a \frac{\partial^2}{\partial r^2}(\rho_p r) \tag{S10}$$

We next introduce the following dimensionless variables:

$$U_s = \frac{r}{R}\frac{(\rho_{ps} - \rho_{p2})}{(\rho_{p0} - \rho_{p2})} \tag{S11}$$

$$U_f = \frac{\rho_{pf} - \rho_{p2}}{\rho_{p0} - \rho_{p2}} \tag{S12}$$

$$\xi = \frac{r}{R} \tag{S13}$$

$$\tau = \frac{K_a t}{R^2} \tag{S14}$$

where $\rho_1$ and $\rho_2$ are the gas density in the reference and sample cells, and $\rho_0$ is the gas density outside the connected pore volume (the gas has flowed from the reference into sample cells but not into samples), and $\rho_0$ is given by

$$\rho_0 = \frac{V_1\rho_1 + (V_2 - V_b)\rho_2}{V_c} \tag{S15}$$

where $V_1$ is the reference cell volume, $V_2$ is the sample cell volume, $V_b$ is the bulk volume of the sample, $V_c$ is the total void volume of the system minus $V_b$ where $V_c = V_1 + V_2 - V_b$.

If the bulk density of the sample is $\rho_b$ and the total mass of the sample is $M_s$, then the total number of sample particles $N$ is:

$$N = \frac{M_s}{\frac{4}{3}\pi {R_a}^3 \rho_b} \tag{S16}$$

Based on Darcy's law, the gas flow into a sample $Q$ is:

$$Q = -4\pi R^2 \left(k_s \frac{\partial p}{\partial r}\right) N = -\frac{3}{R}\frac{M_s}{\rho_b} k_s \frac{\partial p}{\partial r} \tag{S17}$$

According to mass conservation and in combination with Eq. (S17), for $t > 0$ and $r = R_a$, we have

$$-\frac{3}{R} V_b K_a c_t \phi_f \frac{\partial p}{\partial r} \rho_s = V_c \frac{\partial \rho_f}{\partial t} \tag{S18}$$

Substituting Eq. (1C) into Eq. (S18), the boundary condition of Eq. (S10), for $\xi$ =1, is:

$$-\frac{3}{R} V_b K_a \phi_f \frac{\partial \rho_s}{\partial r} = V_c \frac{\partial \rho_f}{\partial t} \tag{S19}$$

Substituting dimensionless variables into Eq. (S10) yields:

$$\frac{\partial U_s}{\partial \tau} = \frac{\partial^2 U_s}{\partial \xi^2} \tag{S20}$$

By defining parameter $K_c$ as:

$$K_c = \frac{V_c}{V_b \phi_f} \tag{S21}$$

the boundary condition of Eq. (S19) becomes:

$$\frac{\partial U_f}{\partial \tau} = -\frac{3}{K_c}\left(\frac{\partial U_s}{\partial \xi} - \frac{U_s}{\xi}\right) \tag{S22}$$

From Eq. (S21), $K_c$ represents the ratio of gas storage capacity of the total void volume of system to the pore volume (including both adsorption and non-adsorption volume) of sample.

The initial condition of Eq. (S20), for $\tau = 0$, is:

$$0 \leq \xi < 1, U_s = 0 \tag{S23}$$

For $\tau > 0$:

$$\xi = 0, U_s = 0 \tag{S24}$$

$$\xi = 1, U_s = U_f = 1 \tag{S25}$$

$$\frac{\partial U_s}{\partial \tau} = \frac{\partial^2 U_s}{\partial \xi^2}, 0 < \xi < 1 \tag{S26}$$

Replacing the Heaviside operator $p = \partial/\partial\tau$ as $p = -s^2$, Eq. (S20) and Eq. (S22) then become:

$$\frac{\partial^2 U_s}{\partial \xi^2} + s^2 U_s = 0\Big|_{U_s=0,\xi=0} \tag{S27}$$

$$\alpha^2(U_s - 1) = \frac{3}{K_c}\left(\frac{\partial U_s}{\partial \xi} - \frac{U_s}{\xi}\right)\Big|_{\xi=1} \tag{S28}$$

For these first- and second-order ordinary differential equations, we can solve Eqs. (S27) and (S28) as:

$$U_s = \frac{\alpha^2 \sin \alpha \xi}{\frac{3}{K_c}(\sin \alpha - \alpha \cos \alpha) + \alpha^2 \sin \alpha} \tag{S29}$$

In Eq. (S29), $\alpha_n$ are the roots of Eq. (S30):

$$\tan \alpha = \frac{3\alpha}{3 + \alpha^2 K_c} \tag{S30}$$

Defining the numerator and denominator of Eq. (S29) as functions $f(\alpha)$ and $F(\alpha)$, $U_s$ can be expressed as:

$$U_s = \underset{\alpha \to 0}{F} \frac{f(\alpha)}{F(\alpha)} + 2 \sum_{n=1}^{\infty} \frac{f(\alpha_n)}{\alpha_n F'(\alpha_n)} e^{-\alpha_n{}^2 \tau} \tag{S31}$$

**S2.1: Solution for the Limited $K_c$ Value**

Under the condition of limited $K_c$ value, Eq. (S20) is solved with the boundary condition of $0 < \xi < 1$ at time $t$, and the gas state on the grain surface is initially at equilibrium with the gas outside. Using the Laplace transform, Eq. (S31) is given as (the Laplace transform part can be found in APPENDIX V of Carslaw & Jaeger, 1959) (Carslaw and Jaeger, 1959):

$$U_s = \frac{\xi K_c}{K_c + 1} + 6 \sum_{n=1}^{\infty} \frac{\sin \xi \alpha_n}{\sin \alpha_n} \frac{K_c e^{-\alpha_n{}^2 \tau}}{9(K_c + 1) + \alpha_n{}^2 K_c{}^2} \tag{S32}$$

As the pressure transducer detects the pressure in the reference cell, with the boundary condition $U_f = U_s|_{\xi=1}$, we can calculate $U_f$ as:

$$U_f = \frac{K_c}{1 + K_c} + 6 \sum_{n=1}^{\infty} \frac{K_c e^{-\alpha_n{}^2 \tau}}{9(K_c + 1) + \alpha_n{}^2 K_c{}^2} \tag{S33}$$

For a convenient expression of $\alpha_n$ through logarithmic equation, Eq. (S33)

can be transformed as:

$$(1-U_f)(1+K_c) = 1 - 6\sum_{n=1}^{\infty} \frac{K_c(1+K_c)e^{-\alpha_n{}^2\tau}}{9(K_c+1)+\alpha_n{}^2K_c{}^2} \tag{S34}$$

The left side of Eq. (S34) clearly has a physical meaning for the state of gas transport outside the sample, and we define $(1-U_f)(1+K_c)$ as $F_f$, which is less than, but infinitely close to, 1. Parameter $F_f$ represents (1) the fraction of final gas transfer of $V_c$ which has taken place by time *t*, which can be interpreted as the net change in the density of gas at time *t* to time infinity as Eq. (S35), or (2) as the fractional approach of the gas density to its steady-state in terms of dimensionless variables as Eq. (S36).

$$F_f = \frac{\rho_{p0} - \rho_{pf}}{\rho_{p0} - \rho_{f\infty}} \tag{S35}$$

or

$$F_f = \frac{1-U_f}{1-U_\infty} = \frac{\rho_{p0} - \rho_{pf}}{\rho_{p0} - \rho_{p2}}(1+K_c) \tag{S36}$$

where for $\tau \to \infty$, the result of $U_f$ and $\rho_{f\infty}$would tend to be the limiting value:

$$U_\infty = U_s = U_f\xi = \left.\frac{\xi K_c}{1+K_c}\right|_{\xi=1} \tag{S37}$$

$$\rho_{f\infty} = \frac{V_1\rho_1 + (V_2 - V_s)\rho_2}{V_1 + V_2 - V_s} = \frac{K_c}{1+K_c}\left(\rho_{p0} - \rho_{p2}\right) + \rho_{p2} \tag{S38}$$

Thus, Eq. (S34) can be expressed as:

$$F_f = 1 - 6\sum_{n=1}^{\infty} \frac{K_c(1+K_c)e^{-\alpha_n{}^2\tau}}{9(K_c+1)+\alpha_n{}^2K_c{}^2} \tag{S39}$$

For calculating the permeability, Eq. (S39) can be linearized as a function of time as there are no variables other than the exponential part:

$$ln(1-F_f) = f_1 - s_1 t \tag{S40}$$

where $f_1$ is the intercept for the y-axis of function (S40):

$$f_1 = ln[\frac{6K_c(1+K_c)}{9(1+K_c)+\alpha_1{}^2K_c{}^2}] \tag{S41}$$

The slope $s_1$ can be captured by the fitted line of the linear segment, and $\alpha_1$ is the first solution of Eq. (S30):

$$s_1 = \frac{\alpha_1{}^2K_a}{R_a{}^2} \tag{S42}$$

Thus, the permeability can be calculated as:

$$k = \frac{R_a{}^2\mu c_t\phi_f s_1}{\alpha_1{}^2} \tag{S43}$$

**S2.2: Solution for $K_c$ Goes to Infinity**

When $V_c$ has an infinite volume compared to the void volume in a sample, which means that the density of gas in $V_c$ would be kept at $\rho_{p0}$, and $\alpha$ would approach $n\pi$ in Eq. (S30), then Eq. (S32) can be transformed as:

$$U_s = \xi + \frac{2}{\pi}\sum_{n=1}^{\infty}(-1)^n \frac{sin\, n\, \pi\xi}{n} e^{-(n\pi)^2\tau} \tag{S44}$$

In this situation, $U_f = 1$, and as the gas density would be maintained at the initial state at $\rho_{p0}$, it would be a familiar case in diffusion kinetics problems with the uptake rate of $F_f$ to be expressed as $F_s$ in $V_b$ (Barrer, 1941):

$$F_s = \frac{\rho_{s\mathrm{av}}}{\rho_{s\infty}} \tag{S45}$$

where $\rho_{s\mathrm{av}}$ is the average value of $\rho_{sr}$ in the grain, and $\rho_{s\infty}$ is the maximum value of $\rho_{sr}$:

$$\rho_{sr} = \rho_{ps} - \rho_{p2},\ \ \rho_{s\infty} = \rho_{p0} - \rho_{p2} \tag{S46}$$

The value of $\rho_{sr}$ in the grain is:

$$\rho_{sav} = \frac{3}{R^3}\int_0^R \rho_{sr} r^2\, d\, r \tag{S47}$$

Then $F_s$ becomes:

$$F_s = \frac{3}{R^3}\int_0^R \frac{U_s}{\xi} r^2\, d\, r \tag{S48}$$

Substituting Eq. (S44) into Eq. (S48), we can calculate:

$$F_s = 1 - \frac{6}{\pi^2}\sum_{n=1}^{\infty}\frac{e^{-(n\pi)^2\tau}}{n^2} \tag{S49}$$

Similar to Eq. (S39), Eq. (S49) can also be linearized to calculate the permeability in $\tau$ from the fitted slope. For $\tau \geq 0.08$, Eq. (S49) can be

reduced as:

$$F_s = 1 - \frac{6}{\pi^2} e^{-\pi^2 \tau} \tag{S50}$$

When $t$ is small enough (for $\tau \leq 0.002$), Eq. (S49) can be transformed into Eq. (S51).

$$F_s = 6\sqrt{\frac{\tau}{\pi}} \tag{S51}$$

As $F_s$ is a special solution of $F_f$ with the case of $K_c$ goes to infinity, we can arrive at:

$$F_s = F_f = \left(1 - U_f\right)(1 + K_c) \tag{S52}$$

For testing the ultra-low permeability rocks using granular samples when $K_c$ goes to infinity, Eq. (S50) and Eq. (S51) can be selected using different $\tau$ values.

From the fitted slope $s_2$ of function $ln(1 - F_s)$ from Eq. (S50), we can then derive the permeability:

$$k = \frac{{R_a}^2 \mu c_t \phi_f s_2}{\pi^2} \tag{S53}$$

The results of Eq. (S53) are very similar to Eq. (S43) as the first solution for Eq. (S30) is very close to $\pi$.

From the fitted slope $s_3$ of function ${F_s}^2$ from Eq. (S51), we can derive the permeability:

$$k = \frac{\pi {R_a}^2 \mu c_t \phi_f s_3}{36} \tag{S54}$$

## S3. A Case of Data Processing for GPT

We show here an illustration of the data processing procedure for the GPT with a molecular sieve sample (https://www.acsmaterial.com/molecular-sieves-5a.html). This material consists of grains of 2 mm in Diameter with a porosity of 26.28%, and a uniform pore-throat size of 5Å in Diameter, with a particle density of 2.96 g/cm$^3$. For a 45 g sample, the $K_c$ value is 19.4 from Eq. (S21), and therefore 4.9% of the density ratio $(1 - K_f)$ is available for mass transfer from Eq. (4).

The experimental data were captured under a strict temperature control and unitary-gas environment, along with a precise measurement of barometric pressure. The experiment was run twice, and after the data were collected, 1) we made a rough evaluation of the "Penetration Zone" of this sample based on Figs. 5-6. For this molecular sieve sample, the "Penetration Zone" is shown in Fig. S1, and the mass transfer in unit time more conforming to a linear state (shown as Fig. 5) over a large time range, especially at 100-300s; 2) data in the selected range (100-300s) were fitted respectively for the slope from Fig. S2, then slopes were compiled in Table S1; 3) permeabilities were calculated using the slope of the fitted curve, and all results for LLT, ILT and IET are also shown in Table S1; 4) the results were checked with their dimensionless times

to verify whether the early- or late-time solutions were used correctly. Table S1 clearly shows that the results of IET should be selected for this sample, as the dimensionless time is less than 0.024. Note that the data fluctuation shown here was from a high resolution ($\pm$0.1% for 250 psi) pressure sensor without undergoing a smoothing process; meanwhile, for data in the 100-200, 200-300, and 300-400 seconds of experimental duration, 100, 200, and 300 seconds respectively were used to calculate the dimensionless times for the results in Table S1.

In addition, the validity of the permeability obtained needs to be verified by using the time interval employed in data fitting and the calculated permeability results to calculate the $\tau$ (Table S1). If the dimensionless time is less than 0.024 (as occurred for the case of molecular sieve), the IET solution is selected; if the dimensionless time is greater than 0.024 and $K_c$ is greater than 10, the ILT solution is used; if $\tau$ is greater than 0.024 and $K_c$ is less than 10, then the LLT solution is employed. However, for sample sizes smaller than 1.27 mm, Conflicting Results (described in Table 1) occur, and results from this situation are not recommended due to poor data quality.

Table S1. Permeability results of molecular sieve from LLT, IET and ILT

| Fitting range (s) | LLT ($m^2$) | $\tau$ - LLT | IET($m^2$) | $\tau$ - IET | ILT ($m^2$) | $\tau$ -ILT | Slope-LLT | Slope-IET | Slope-ILT |
|---|---|---|---|---|---|---|---|---|---|
| 100-200 | 5.60E-22 | 0.004 | 1.02E-21 | 0.007 | 5.00E-22 | 0.003 | 0.0004 | 0.0007 | 0.0004 |
| 200-300 | 4.20E-22 | 0.006 | 5.81E-22 | 0.008 | 3.75E-22 | 0.005 | 0.0003 | 0.0004 | 0.0003 |
| 300-400 | 2.80E-22 | 0.006 | 4.36E-22 | 0.009 | 2.50E-22 | 0.005 | 0.0002 | 0.0003 | 0.0002 |

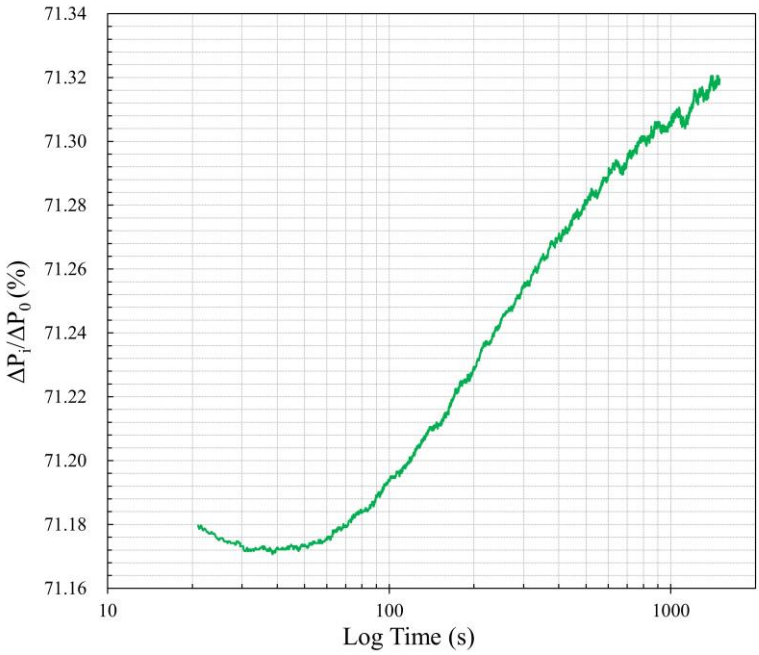


Fig. S1. Unit pressure changes vary with experimental time.

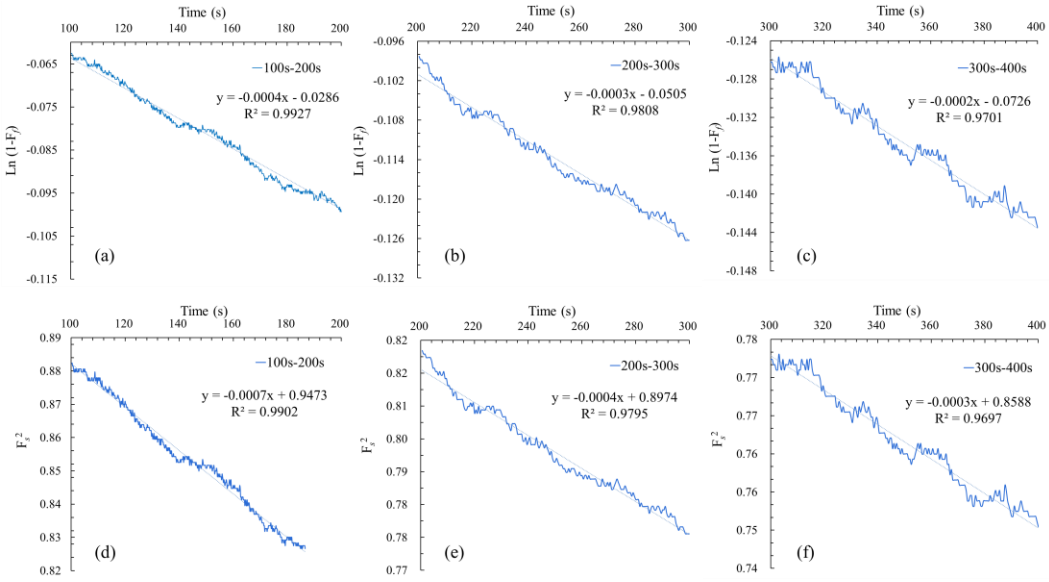


Fig. S2. Fitted slopes for each solution; (a) to (c) are results of LLT and ILT, while (d) to (f) of IET.

## S4. Equipment and samples

The experimental setup in the GPT presented in this study is based on the GRI-95/0496 protocols (Guidry et al., 1996) and the SMP-200 guidelines from Core Laboratories with the gas expansion approach (shown in Fig. S3). In this work, gases (He, Ar, $N_2$, or $CO_2$) with different molecular sizes and sorption capacities were tested using two shale core samples (X1, X2) from an oil-producing lacustrine formation in the Songliao Basin, China. X1 is used for sample size study where X2 is used for experiment with different gas. Also, we used the molecular sieve to exhibit the practical utilization of the GPT method in SI C. We gently crushed the intact samples with mortar and ground to different granular sizes from 0.34 mm to 5.18 mm through a stack of sieves (named here as Size X: 8 mm to #8 mesh; GRI+: #8-#12 mesh; Size A: #12-#20 mesh; GRI: #20-#35 mesh; Size B: #35-#80 mesh).

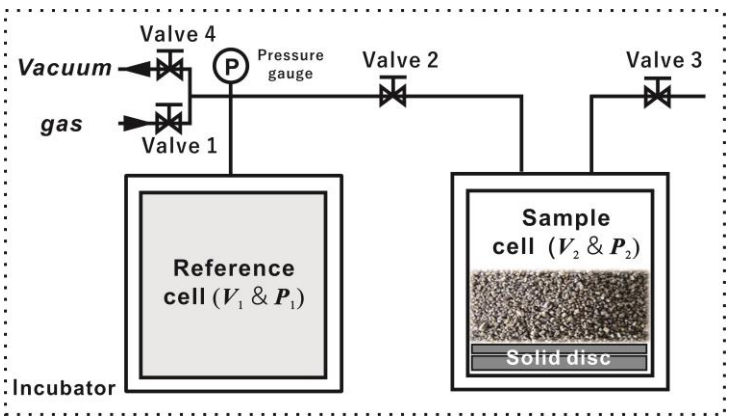


Fig. S3. Scheme of the GPT experiment for granular samples with all the cells and supplies placed inside an incubator for temperature control.

After loading each sample, related accessories (e.g., solid discs or balls for volume control; and hence porosity, sample mass, and solution-related) were placed below samples inside the cell (Fig. S3). Next, valves 1 and 3 were closed, then valves 2 and 4 were opened for air evacuation. Using a precise pressure gauge connected to the reference cell shown in Fig. S3 we monitored changes in the pressure. The evacuation time typically lasted at least 15-30 min, and then the system was allowed to stabilize for another 15 min. As the moisture content of the samples significantly influences the final vacuum, the samples were placed into the sample cell immediately after removal from the drying oven set at 60$^{o}$C for two days and cooling in a low-humidity desiccator.

The experiments were conducted at the temperature of 35°C by placing the SMP-200 inside an incubator equipped with a high precision temperature-humidity sensor to monitor changes. This is to ensure that the system temperature was always stable (0.05°C over at least 45 mins of experimental duration). For temperature monitoring, after evacuation, we closed valves 3 and 4 followed by opening valves 1 and 2 (shown in Fig. S3) and monitoring the heat convection and conduction in the system with the pressure gauge. Normally, the sample was placed inside the sample cell in less than 30 sec after opening the incubator and remained at least 45 min for the gas pressure to stabilize before the pressure decay test. After the pressure was stabilized

(0.005 psi for an experimental pulse pressure of 200 psi), it was deemed that there was no appreciable additional flow due to temperature variation in the system, as indicated by the rebound of the pressure decay curve. After reaching a unitary gas condition and stable temperature in the GPT experiment, valves 2 and 4 were closed, and the reference cell was filled with the probing gas (mostly non-reactive helium) at 200 psi. Valve 2 was then opened to release the pressure in the reference cell into the void volume in the sample cell, and the pressure decay for both reference and sample cells were recorded over time.

## S5. Experimental conditions

We performed leakage tests by measuring the pressure variation with non-porous solids, such as steel balls, as any leakage would cause pressure variations and, accordingly, errors in permeability measurements of tight porous samples (Heller et al., 2014). Before the data from porous samples were analyzed, the leakage pressure from the steel ball experiment was subtracted from the sample data to correct the modest (<5% of the pressure levels used for permeability analyses) leakage effect.

The need for a unitary gas environment (a single gas used in both reference and sample cells) is needed to successfully measure permeability via the GPT method. The relative movement of gas molecules in the mass transfer process is driven by the gas density gradient in the system. During gas transport, the

pressure variance was recorded and used to obtain the permeability coefficient. However, when the gas in both cells is different, e.g., helium in the reference and air in the sample cells, the mathematical analysis requires a complicated correction accounting for the mean molar mass and the average gas dynamic viscosity of the gas mixture. In this study, we present the calculation with the viscosity of mixed gases for the GPT in SI A. Since the mixed gas environment is not recommended, air evacuation should be used for a well-controlled unitary gas environment in the GPT.

A stable temperature is another critical point to ensure the success of the GPT experiment. A sensitive pressure transducer in combination with the ideal gas law, used to establish the relationship between pressure and gas volume change, would be a much more convenient and precise way than the gas flow meter to determine the gas permeability considering the measurement accuracy. According to Amonton's law (Gao et al., 2004), the kinetic energy of gas molecules is determined by the temperature, and any changes would alter the molecular collision force causing a pressure variation and a volumetric error. The GPT experiments were run two or three times on the same sample, and the sample skeletal density at the end of the experiment were obtained to check the overall indication of leakage and temperature control. The experimental data with relatively large and stable skeletal density (mostly

the last run, from small but appreciable pressure change to reach stable values) were used.

## SI References


Barrer, R. M.: Diffusion in and Through Solids, Рипол Классик, 1941.

Brokaw, R. S.: Viscosity of Gas Mixtures, National Aeronautics and Space Administration, 1968.

Carslaw, H. S., and Jaeger, J. C.: Conduction of Heat in Solids, 1959.

Gao, J., Luedtke, W. D., Gourdon, D., Ruths, M., Israelachvili, J. N., and Landman, U.: Frictional forces and Amontons' law: From the molecular to the macroscopic scale., ACS Publications, 2004.

Guidry, K., Luffel, D., and Curtis, J.: Development of laboratory and petrophysical techniques for evaluating shale reservoirs. Final technical report, October 1986-September 1993., ResTech Houston, Inc., TX (United States), 1996.

Haskett, S. E., Narahara, G. M., and Holditch, S. A.: A method for simultaneous determination of permeability and porosity in low-permeability cores, SPE Formation Evaluation, 3, 651-658, 1988.

Heller, R., Vermylen, J., and Zoback, M.: Experimental investigation of matrix permeability of gas shales, AAPG Bulletin, 98, 975-995, 2014.

Sutherland, W.: XXXVII. The viscosity of mixed gases, The London, Edinburgh, and Dublin Philosophical Magazine and Journal of Science, 40, 421-431, 1895.